Springer

KSME

Journal of Mechanical Science and Technology 29 (11) (2015) 4601~4610
www.springerlink.com/content/1738-494x(Print)/1976-3824(Online)
DOI 10.1007/s12206-015-1005-1

Forced response of the inertial piezoelectric rotary motor to electric excitation †

Lizhong Xu* and Jichun Xing

School of Mechanical Engineering, Yanshan University, China

(Manuscript Received January 20, 2015; Revised April 5, 2015; Accepted July 16, 2015)

Abstract

For a novel inertial piezoelectric rotary motor, the equation of the voltage response on the piezo-ceramic bimorph under the excitation signals is deduced and the dynamic equation of the motor rotor is given. Using the equations, the voltage responses on the piezo-ceramic bimorph and the responses of the displacement, velocity and acceleration on the rotor to the sawtooth voltage excitation are investigated. The results show that when the frequency of the excitation signal is quite low, the waveform of the displacement response of the rotor is identical to one of the excitation signal; the outer diameter of the rotor, its length and thickness, etc., have obvious effects on the inertial moment applied to the rotor. The results are useful for design and control of the operating performance of the motor.

Keywords: Forced response; Inertia torque; Piezoelectric motor; Saw-tooth wave

1. Introduction

Piezoelectric motors maintain relatively high torque at relatively low speeds, without a reduction gear [1, 2]. They have been commercially employed for automated focusing systems of cameras and X-Y positioning systems [3]. There are two kinds of the piezoelectric motors: the rotational motor and the linear motor. As a linear type motor, an inertial drive motor has an advantage due to its simple construction. One of the inertial motors is an impact drive mechanism driven by impulse inertial force [4]. Using the mechanism, micromanipulator for cell manipulation, and auxiliary positioning system for Scanning tunneling microscopy (STM) and Atomic force microscope (AFM) were developed [5, 6]. Another inertial drive is the smooth impact drive mechanism. Here, a base plate or bar is driven with rapid expansion and slow shrinkage. The slider on the base slips during rapid motion and follows the base due to frictional force. With this principle, many applications have been proposed and fabricated [7-9]. The rotational motor includes standing wave type ultrasonic motors and traveling wave ultrasonic motors. The standing wave motors have simpler construction than traveling wave ones [10]. The traveling wave motors represent a main generation of motors which are suited for many applications [11-13].

The structure of the rotational motors is relatively complicated and further miniaturization is difficult. Authors proposed a novel inertial piezoelectric rotary motor in Ref. [14]. The motor structure is so simple that the further miniaturization of the rotational motor can be done easily. As shown in Fig. 1, the novel inertial rotary motor consists of a stator and a rotor. The rotor includes an outer ring, an inner ring, and two ribs connecting the outer ring to the inner ring. The inner ring is mounted on a supporting bearing and the outer ring is used as the inertial mass. The piezo-ceramic bimorph is adhibited on each side surface of the two ribs. As soon as a rapid rise input voltage is supplied to the motor, it excites the transverse bending vibration mode of the two ribs. Thus, inertial forces within the outer ring occur, which causes an inertial torque applied to the rotor and make it rotate. Then, a slow decreasing input voltage is supplied to the motor, so the inertial forces within the outer ring are so small that the inertial torque can be balanced by the friction torque between the rotor and the bearing. Thus, the rotor does not rotate. The rapid increasing and slow decreasing input voltage with a special frequency is supplied to the motor periodically, and then the rotor can rotate continuously. In Fig. 1(b) is the effective width of the beam, h the thickness of the beam, R_1 and R_2 are the inter and outer diameters of the rotor, respectively, L_p is the length of the piezo-ceramic bimorph.

The working principle of the motor was elucidated, the model machine was manufactured [14], and its output torque was analyzed [15]. However, the forced response of the motor to the electric excitation has not been investigated yet. The inertial moment applied to the rotor has not been determined yet. It is unfavorable to design the load-carrying ability of the motor.

In this paper, from the driving circuit equation of the motor,

*Corresponding author. Tel.: +86 3358061472, Fax.: +86 3358074783
E-mail address: xlz@ysu.edu.cn
† Recommended by Associate Editor Ohseop Song

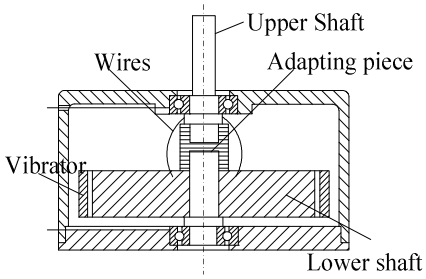

(a) Motor structure

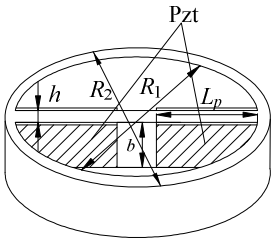

(b) Rotor structure

Fig. 1. Motor and rotor structure.

the equation of the voltage response on the piezo-ceramic bimorph to the excitation signals is determined. The equation of the strain energy in the piezo-ceramic bimorph, the equations of the strain energy and the kinetic energy in the rotor beam are given. Substituting these energy equations into Lagrange equation, the dynamic equation of the rotor is obtained. Using these equations, the responses of the voltage on the piezo-ceramic bimorph and the responses of the displacement, velocity and acceleration on the rotor to the sawtooth voltage excitation are investigated. The effects of the system parameters on the responses are analyzed. The condition to make the motor rotate in one direction is discussed. The results show that the same waveform of the voltage response on the piezo-ceramic bimorph as one of the excitation signal can be obtained when the frequency of the excitation signal is much smaller than the first order natural frequency of the rotor. When the frequency of the excitation signal is quite low, the waveform of the displacement response of the rotor is identical to one of the excitation signal. As the frequency of the excitation signal grows, the waveform of the displacement response becomes more different from one of the excitation signal. The outer diameter of the rotor, its length and thickness, etc have obvious effects on the inertial moment applied to the rotor. The results are useful for design and control of the operating performance of the motor.

2. Voltage excitation

For the motor motion, a voltage excitation with sawtooth wave is applied to the piezo-ceramic bimorph (see Fig. 2). Here, t is the time, T is the period of the excitation signal, $\mu(0 < \mu < 1)$ is the ratio of the rise time to the period, A is the peak voltage. The voltage excitation can be written by

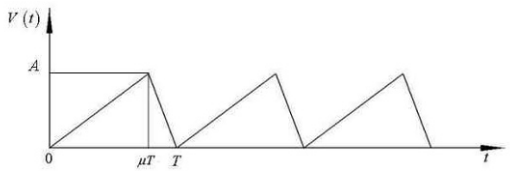

Fig. 2. Applied electrical signal wave.

$$V(t)=\begin{cases}\dfrac{A}{\mu T}t & (0\le t<\mu T)\\ \dfrac{A}{(\mu-1)T}t+\dfrac{A}{1-\mu} & (\mu T\le t\le T)\end{cases}. \tag{1}$$

The piezo-ceramic bimorph can be considered as an equivalent capacitance. Thus, the driving circuit equation of the motor can be given as

$$V-V_R-V_C=0, \tag{2}$$

where V is the excitation voltage, V_R is the voltage on the resistance ($V_R = iR$, i is the current, $i = dq/dt$, q is quantity on the piezo-ceramic bimorph and R is the resistance), V_C is the voltage on the piezo-ceramic bimorph($V_C=\frac{1}{C}\int_0^t idt$, C is the capacitance).

Substituting Eq. (1) and related equations into Eq. (2), yields

$$\frac{dq}{dt}+\frac{1}{RC}q=\frac{A}{\mu TR}t \qquad (0\le t<\mu T), \tag{3a}$$

$$\frac{dq}{dt}+\frac{1}{RC}q=-\frac{A}{(1-\mu)TR}t+\frac{A}{(1-\mu)R}$$

$$(\mu T\le t\le T). \tag{3b}$$

The initial condition is $q(0) = 0$. From Eq. (3a), it is known

$$V_c=\frac{q}{C}=\frac{A}{\mu T}\left(RCe^{\frac{-t}{RC}}-RC+t\right). \tag{4}$$

Let $t = \mu T$, Eq. (4) can give the initial condition of the Eq. (3b) as below:

$$q(\mu T)=\frac{A}{\mu T}\left(RCe^{\frac{-\mu T}{RC}}-RC+\mu T\right). \tag{5}$$

Thus, the solution of the Eq. (3b) is

$$V_c=\frac{q}{C}=\frac{A}{\mu T}RC\left(1-\frac{1}{(1-\mu)}e^{\frac{\mu T}{RC}}\right)e^{\frac{-t}{RC}}+\frac{A(RC+T-t)}{(1-\mu)T}. \tag{6}$$

In the same manner, the voltage V_C for any rise excitation voltage can be given as

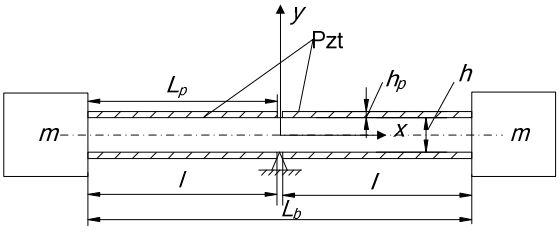

Fig. 3. Dynamics model of the rotor.

$$V_c = \frac{ARC}{\mu T}\varsigma_n e^{\frac{-t}{RC}} + \frac{A}{\mu T}\left(t-(n+1)T-RC\right)$$
$$(n+1)T \le t \le (n+1)T+\mu T \quad (n=1,2,3\cdots), \tag{7a}$$

where

$$\varsigma_n = \left(1-\frac{1}{(1-\mu)}e^{\frac{\mu T}{RC}} + \sum_{i=1}^{n+1}\frac{1}{(1-\mu)}e^{\frac{nT}{RC}} - \sum_{i=1}^{n}\frac{1}{(1-\mu)}e^{\frac{(n+\mu)T}{RC}}\right).$$

The voltage V_C for any trailing edge of the excitation voltage can be given as

$$V_c = \frac{ARC}{\mu T}\varsigma_n e^{\frac{-t}{RC}} + \frac{A\left(RC+(n+1)T-t\right)}{(1-\mu)T}$$
$$nT+\mu T \le t \le (n+1)T \quad (n=1,2,3\cdots). \tag{7b}$$

3. Forced responses

For simplifying the analysis, the rotor of the motor is considered as a beam with inertial mass at its two ends (see Fig. 3). From the model, the dynamics equation of the rotor can be given as follows:

$$EI\frac{\partial^4 y(x,t)}{\partial x^2} + C_d\frac{\partial y(x,t)}{\partial t} + \rho_l\frac{\partial^2 y(x,t)}{\partial t^2} = 0, \tag{8}$$

where $y(x,t)$ is transverse displacement of the beam, x is length coordinate of the beam, ρ_l is material density per unit length of the beam, E is modulus of elasticity of the beam material, $I = bh^3/12$, it is the second moment of area of the beam, L_b is the length of the rotor, C_d is the damping coefficient.

The transverse displacement of the beam can be given as [16]

$$y(x,t) = \sum_{i=1}^{\infty}\phi_i(x)q_i(t), \tag{9}$$

where $\phi_i(x)$ is the mode function,

$$\phi_i(x) = \sin\beta_i x - \frac{-\cos\beta_i l + \alpha\beta_i l\sin\beta_i l}{\mathrm{ch}\,\beta_i l + \alpha\beta\, l\,\mathrm{sh}\,\beta_i l}\mathrm{sh}\beta_i x, \quad (i=1,2\cdots).$$

It is obtained from the boundary condition of the central support beam such as shown in Fig. 3; $q_i(t)$ is the time function.

From piezoelectric equation, the stress in the piezo-ceramic bimorph is [17]

$$\sigma_1(x,t) = -e_{31}E_3 + c_{11}^E\varepsilon,$$

where E_3 is the electric-field intensity on the piezo-ceramic bimorph, e_{31} is the piezoelectric stress constant, c_{11}^E is the stiffness constant, ε is the strain.

The piezo-ceramic bimorph is adhibited on each side surface of the beam; the strain in the piezo-ceramic bimorph can be calculated as

$$\varepsilon = \frac{h}{2}\frac{\partial^2 y(x,t)}{\partial x^2}. \tag{10}$$

Substituting Eq. (10) into piezoelectric equation, yields

$$\sigma_1(x,t) = -e_{31}E_3 + \frac{h}{2}c_{11}^E\frac{\partial^2 y(x,t)}{\partial x^2}, \tag{11}$$

where $E_3(x,t) = \frac{V_c(x)}{h_p}$, h_p is the thickness of the piezo-ceramic bimorph.

The strain energy in the piezo-ceramic bimorph is

$$U_p = \frac{b}{2}\int_0^{L_p}\sigma_1(x,t)\varepsilon_1 dx. \tag{12}$$

Substituting Eqs. (10) and (11) into Eq. (12), yields

$$U_p = \frac{bh}{4}\sum_{i=1}^{\infty}q_i(t)\int_0^{L_p}-e_{31}E_3\phi''(x)dx + \frac{1}{2}\sum_{i=1}^{\infty}k_{ij}^p q_i(t)q_j(t) \tag{13}$$

where $k_{ij}^p = k_{ji}^p = \int_0^{L_p}\frac{bh^2}{4}c_{11}^E\phi_i''(x)\phi_j''(x)dx$.

The strain energy in the rotor beam is

$$U_{L/P} = \frac{1}{2}\int_0^l EI\left[\frac{\partial^2 y(x,t)}{\partial x^2}\right]^2 dx = \frac{1}{2}\sum_{i=1}^{\infty}\sum_{j=1}^{\infty}k_{ij}^l q_i(t)q_j(t) \tag{14}$$

where $k_{ij}^l = k_{ji}^l = \int_{-l}^{l}EI\phi_i''(x)\phi_j''(x)dx$, l is the length of the rotor beam.

The four piezo-ceramic bimorphs are used in the motor, so the total strain energy in the beam and the piezo-ceramic bimorph is

$$U = 4U_p + U_{L\backslash P}. \tag{15}$$

The kinetic energy of the beam is

$$E_m = \frac{1}{2}\int_{-l}^{l}\rho S\left[\frac{\partial y}{\partial t}(x,t)\right]^2 dx = \frac{1}{2}\sum_{i=1}^{\infty}\sum_{j=1}^{\infty} m_{ij}\dot{q}_i(t)\dot{q}_j(t) \tag{16}$$

where

$m_{ij} = m_{ji} = \int_{-l}^{l}\rho S\phi_i(x)\phi_j(x)dx + m\phi_i(-l)\phi_j(-l) + m\phi_i(l)\phi_j(l)$; it is the equivalent mass of the motor rotor, m is the inertial mass.

Considering the damping of the rotor, letting dissipation function as below:

$$D = \frac{1}{2}\sum_{i=1}^{\infty}\sum_{j=1}^{\infty} c_{ij}q_i(t)q_j(t),$$

where $c_{ij} = c_{ji} = \int_{-l}^{l} C_d\varphi_i(x)\varphi_j(x)dx$ is the generalized damping.

Substituting the dissipation function, Eqs. (15) and (16) into Lagrange equation, yields

$$\mathbf{M}\ddot{q}(t) + \mathbf{C}\dot{q}(t) + \mathbf{K} = \mathbf{F}(t), \tag{17}$$

where $\mathbf{M} = \left[m_{ij}\right]$, it is the mass matrix, $\mathbf{K} = \left[k_{ij}\right]$, it is the stiffness matrix, $k_{ij} = k_{ij}^{p} + k_{ij}^{l}$, $\mathbf{F}(t)$ is the generalized force vector, $\mathbf{C} = \left[c_{ij}\right]$, which is the damping matrix, $c_{ij} = c_{ji} = \int_0^l C_d\phi_i(x)\phi_j(x)dx$.

Using the orthogonality of the mode functions, Eq. (17) can be changed into following form uncoupled from each other:

$$\mathbf{M_n}\ddot{q}(t) + \mathbf{C_n}\dot{q}(t) + \mathbf{K_n}q(t) = \mathbf{F_n}(t), \tag{18}$$

where $\mathbf{M_n}$, $\mathbf{C_n}$ and $\mathbf{K_n}$ are the diagonal mass, damping and stiffness matrixes. $\mathbf{F_n}(t) = \left\{\mathrm{F_1}(t)\ \cdots\ \mathrm{F}_i(t)\ \cdots\right\}^T$, the regular force vector.

The each element of the regular force vector is

$$\begin{aligned} F_i(t) &= \frac{bh}{4}\left(2\int_{-l}^{l} e_{31}E_3\delta(x-x_a)\phi_i''(x)dx \right.\\ &\left. +2\int_{-l}^{l} e_{31}E_3\delta(x-x_b)\phi_i''(x)dx\right) \\ &= \frac{bhe_{31}V_c}{2h_p}\left(\phi_i''(x_a) + \phi_i''(x_b)\right) \end{aligned} \tag{19}$$

where x_a and x_b are the average positions of the piezo-ceramic bimorphs.

During $0 \le t < \mu T$, the solution of Eq. (18) is

$$\begin{aligned} q_{1j} &= \frac{F_n}{M_j\omega_{rj}}\int_0^t F_j(\tau)e^{-\xi_j\omega_j(t-\tau)}\sin\omega_{rj}(t-\tau)d\tau \\ &= \frac{F_n}{M_j\omega_{rj}}\frac{A}{\mu T}\frac{1}{\omega_j^4\left(\omega_j^2R^2C^2 - 2\xi_j\omega_jRC + 1\right)} \\ &\left\{\left[\left(2\xi_j^2\omega_j^2 - \omega_j^2\right) + \xi_j\omega_jRC\left(3\omega_j^2 - 4\xi_j^2\omega_j^2\right)\right]\mathrm{e}^{-\xi_j\omega_jt}\sin\omega_{rj}t \right.\\ &+\left[RC\left(\omega_j^2 - 4\xi_j^2\omega_j^2\right) + 2\xi_j\omega_j\right]\omega_{rj}\mathrm{e}^{-\xi_j\omega_jt}\cos\omega_{rj}t \\ &+R^3C^3\omega_{rj}\omega_j^4e^{-\frac{t}{RC}} \\ &\left.-\omega_{rj}\omega_j\left(\omega_j^2R^2C^2 - 2\xi_j\omega_jRC + 1\right)\left(\omega_jRC - \omega_jt + 2\xi_j\right)\right\} \end{aligned} \tag{20}$$

where ω_{rj} is the jth natural frequency of the rotor, $\omega_{rj} = \omega_j\sqrt{1-\xi_j^2}$. $\xi_j = \frac{C_j}{2\omega_j}$, it is the relative damping coefficient.

During $\mu T \le t \le T$, the solution of Eq. (18) is

$$\begin{aligned} q_{2j} &= e^{-\xi_j\omega_j(t-\mu T)}\left[\frac{\dot{q}_{j(\mu T)} + \xi_j\omega_jq_{j(\mu T)}}{\omega_{rj}}\sin\omega_{rj}(t-\mu T)\right. \\ &\left.+q_{(\mu T)}\cos\omega_{rj}(t-\mu T)\right] \\ &+\frac{F_n}{M_j\omega_{rj}}\frac{A}{\mu(1-\mu)T\omega_j^4\left(\omega_j^2R^2C^2 - 2\xi_j\omega_jRC + 1\right)} \\ &\left\{\mathrm{e}^{-(t-\mu T)\xi_j\omega_j}\left\{R^2C^2\omega_j^4\left(1-\xi_j\omega_jRC\right)(1-\mu)\varsigma_0\mathrm{e}^{-\frac{\mu T}{RC}}\right.\right. \\ &-\mu\omega_j^2\left(R^2C^2\omega_j^2 - 2\xi_j\omega_jRC + 1\right) \\ &\left.\left[\xi_j\omega_j\left(RC + (1-\mu)T\right) + \left(2\xi_j^2 - 1\right)\right]\right\}\sin\omega_{rj}(t-\mu T) \\ &+\mathrm{e}^{-(t-\mu T)\xi_j\omega_j}\left\{-R^3C^3\omega_{rj}\omega_j^4(1-\mu)\varsigma_0\mathrm{e}^{-\frac{\mu T}{RC}}\right. \\ &-\mu\omega_{rj}\omega_j\left(R^2C^2\omega_j^2 - 2\xi_j\omega_jRC + 1\right) \\ &\left.\left\{\omega_j\left[RC + (1-\mu)T\right] + 2\xi_j\right\}\right\}\cos\omega_{rj}(t-\mu T) \\ &+(1-\mu)R^3C^3\omega_{rj}\omega_j^4\varsigma_0\mathrm{e}^{-\frac{t}{RC}} \\ &\left.+\mu\omega_{rj}\omega_j\left(\omega_j^2R^2C^2 - 2\xi_j\omega_jRC + 1\right)\left(RC\omega_j - \omega_j(t-T) + 2\xi_j\right)\right\} \end{aligned} \tag{21}$$

During $(n+1)T \le t \le (n+1)T+\mu T$ (n = 1,2,3$\cdots$) , the solution of Eq. (18) is

$$\begin{aligned} q_{(2n-1)j} &= e^{-\xi_j\omega_j(t-nT)}\left[\frac{\dot{q}_{j(nT)} + \xi_j\omega_jq_{j(nT)}}{\omega_{rj}}\sin\omega_{rj}(t-nT)\right. \\ &\left.+q_{(nT)}\cos\omega_{rj}(t-nT)\right] \\ &+\frac{F_n}{M_j\omega_{rj}}\frac{A}{\mu T}\frac{1}{\omega_j^4\left(\omega_j^2R^2C^2 - 2\xi_j\omega_jRC + 1\right)} \\ &\left\{\mathrm{e}^{-(t-nT)\xi_j\omega_j}\left[R^2C^2\omega_j^4\left(-\xi_j\omega_jRC + 1\right)\zeta_n\mathrm{e}^{-\frac{nT}{RC}}\right.\right. \\ &+\left(\xi_j\omega_jRC - 1 + 2\xi_j^2\right)\omega_j^2 \\ &\left.\left.\left(\omega_j^2R^2C^2 - 2\xi_j\omega_jRC + 1\right)\right]\sin\omega_{rj}(t-nT)\right. \end{aligned} \tag{22}$$

$$+\mathrm{e}^{-(t-nT)\xi_j\omega_j}\left[-R^3C^3\omega_{rj}\omega_j^4\zeta_n\mathrm{e}^{-\frac{nT}{RC}}\right.$$
$$+\omega_{rj}\omega_j\left(RC\omega_j+2\xi_j\right)$$
$$\left.\left(\omega_j^2R^2C^2-2\xi_j\omega_jRC+1\right)\right]\cos\omega_{rj}\left(t-nT\right)$$
$$+R^3C^3\omega_{rj}\omega_j^4\zeta_n\mathrm{e}^{-\frac{t}{RC}}-\omega_{rj}\omega_j\left(\omega_j^2R^2C^2-2\xi_j\omega_jRC+1\right)$$
$$\left.\left(RC\omega_j-\omega_j\left(t-nT\right)+2\xi_j\right)\right\}$$

where

$$\varsigma_n=\left(1-\frac{1}{(1-\mu)}e^{\frac{\mu T}{2RC}}+\sum_{i=1}^{n+1}\frac{1}{(1-\mu)}e^{\frac{(2n-\mu)T}{2RC}}-\sum_{i=1}^{n}\frac{1}{(1-\mu)}e^{\frac{(2n+\mu)T}{2RC}}\right).$$

During $nT+\mu T\le t\le(n+1)T$ (n = 1,2,3⋯), the solution of Eq. (18) is

$$q_{2nj}=e^{-\xi_j\omega_j\left[t-(nT+\mu T)\right]}\left\{\frac{\dot{q}_{j(nT+\mu T)}+\xi_j\omega_jq_{j(nT+\mu T)}}{\omega_{rj}}\right.$$
$$\left.\sin\omega_{rj}\left[t-\left(nT+\mu T\right)\right]+q_{(nT+\mu T)}\cos\omega_{rj}\left[t-\left(nT+\mu T\right)\right]\right\}$$
$$+\frac{F_n}{M_j\omega_{rj}}\frac{A}{\mu(1-\mu)T\omega_j^4\left(\omega_j^2R^2C^2-2\xi_j\omega_jRC+1\right)}$$
$$\left\{\mathrm{e}^{-\left[t-(nT+\mu T)\right]\xi_j\omega_j}\left\{R^2C^2\omega_j^4\left(1-\xi_j\omega_jRC\right)(1-\mu)\varsigma_n\mathrm{e}^{-\frac{nT+\mu T}{RC}}\right.\right.$$
$$-\mu\omega_j^2\left(R^2C^2\omega_j^2-2\xi_j\omega_jRC+1\right)$$
$$\left.\left\{\xi_j\omega_j\left[RC+(1-\mu)T\right]+\left(2\xi_j^2-1\right)\right\}\right\}\sin\omega_{rj}\left(t-\left(nT+\mu T\right)\right)$$
$$+\mathrm{e}^{-\left[t-(nT+\mu T)\right]\xi_j\omega_j}\left\{-R^3C^3\omega_{rj}\omega_j^4(1-\mu)\varsigma_n\mathrm{e}^{-\frac{nT+\mu T}{RC}}\right.$$
$$-\mu\omega_{rj}\omega_j\left(R^2C^2\omega_j^2-2\xi_j\omega_jRC+1\right)$$
$$\left.\left\{\omega_j\left[RC+(1-\mu)T\right]+2\xi_j\right\}\right\}\cos\omega_{rj}\left(t-\left(nT+\mu T\right)\right)$$
$$+(1-\mu)R^3C^3\omega_{rj}\omega_j^4\varsigma_1\mathrm{e}^{-\frac{t}{RC}}+\mu\omega_{rj}\omega_j\left(\omega_j^2R^2C^2-2\xi_j\omega_jRC+1\right)$$
$$\left.\left(RC\omega_j-\omega_j\left(t-2T\right)+2\xi_j\right)\right\} \tag{23}$$

where $\varsigma_n=1-\frac{1}{1-\mu}e^{\frac{\mu T}{2RC}}+\sum_{i=1}^{n}\frac{1}{1-\mu}e^{\frac{(2n-\mu)T}{2RC}}-\sum_{i=1}^{n}\frac{1}{1-\mu}e^{\frac{(2n+\mu)T}{2RC}}$.

During $(n+1)T\le t\le(n+1)T+\mu T$ (n = 1,2,3⋯), the displacement, velocity and acceleration of the motor rotor can be given as

$$y(x,t)=\sum_{j=1}^{\infty}\phi_j(x)q_{(2n-1)j}(t), \tag{24a}$$
$$\dot{y}(x,t)=\sum_{j=1}^{\infty}\phi_j(x)\dot{q}_{(2n-1)j}(t), \tag{24b}$$
$$\ddot{y}(x,t)=\sum_{j=1}^{\infty}\phi_j(x)\ddot{q}_{(2n-1)j}(t). \tag{24c}$$

Table 1. Parameters of the numerical example.

A(V)	μ	R(Ω)	C(nF)
100	0.8	100	2.4

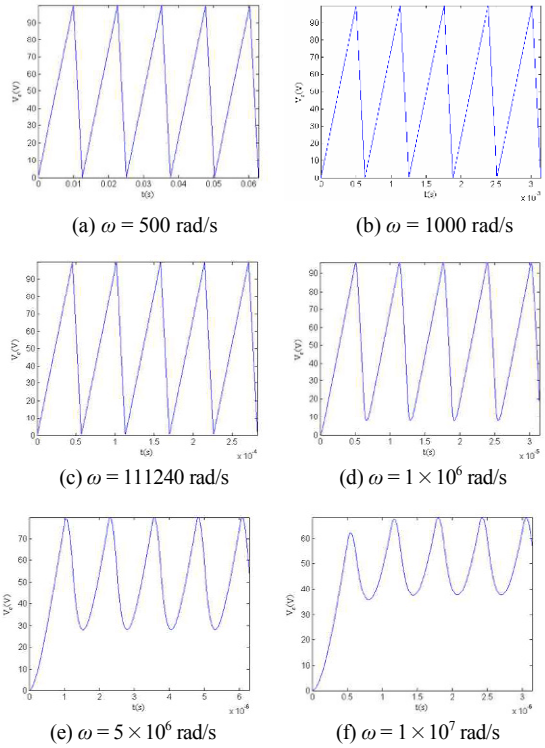

(a) ω = 500 rad/s (b) ω = 1000 rad/s

(c) ω = 111240 rad/s (d) $\omega = 1\times10^6$ rad/s

(e) $\omega = 5\times10^6$ rad/s (f) $\omega = 1\times10^7$ rad/s

Fig. 4. The voltage on piezo-ceramic bimorph under different frequency excitation signals.

Here, $q_{(2n-1)j}(t)$ is calculated from Eq. (22).

During $nT+\mu T\le t\le(n+1)T$ (n = 1,2,3⋯), the displacement, velocity and acceleration of the motor rotor can be given as

$$y(x,t)=\sum_{j=1}^{\infty}\phi_j(x)q_{2nj}(t), \tag{25a}$$
$$\dot{y}(x,t)=\sum_{j=1}^{\infty}\phi_j(x)\dot{q}_{2nj}(t), \tag{25b}$$
$$\ddot{y}(x,t)=\sum_{j=1}^{\infty}\phi_j(x)\ddot{q}_{2nj}(t). \tag{25c}$$

Here $q_{2nj}(t)$ is calculated from Eq. (23).

4. Results and discussion

Eq. (7) is utilized for the voltage analysis on the piezo-ceramic bimorph. The parameters of the numerical example are shown in Table 1. Based on Eq. (7), the voltage response on the piezo-ceramic bimorph to the excitation signals under the different exciting frequencies is given (see Fig. 4). Here, ω is the frequency of the excitation signals. From Fig. 4, the following observations are worth noting:

(1) When the frequency of the excitation signal is smaller than 111240 rad/s (it is the first-order natural frequency of the rotor), considered to be low frequency. When the frequency of the excitation signal is low, the waveform of the voltage response on the piezo-ceramic bimorph is completely identical to one of the excitation signal. However, the peak value of the voltage is slightly smaller than that of the excitation signal.

(2) When the frequency of the excitation signal is high, the waveform of the voltage response on the piezo-ceramic bimorph is different from one of the excitation signal. The peak value of the voltage is much smaller than that of the excitation signal. As the frequency of the excitation signal grows, the peak value of the voltage on the piezo-ceramic bimorph drops obviously and its waveform becomes more different from one of the excitation signal.

(3) When the frequency of the excitation signal is smaller than 111240 rad/s, the waveform of the voltage response on the piezo-ceramic bimorph is identical to one of the excitation signal. The frequency 111240 rad/s is the first-order natural frequency of the rotor. Hence, the frequency of the excitation signal should be smaller than the first-order natural frequency of the rotor to obtain the same waveform of the voltage response on the piezo-ceramic bimorph as one of the excitation signal.

Eqs. (22)-(25) are utilized for the response analysis of the rotor to pulse voltage signals. The parameters of the numerical example are shown in Table 2. Based on Eqs. (24) and (25), the displacement and acceleration responses of the rotor end to voltage excitation signals are investigated (see Fig. 5). From Fig. 5, we know:

(1) The displacement response of the rotor end to the excitation signals is similar to the voltage response on the piezo-ceramic bimorph. When the frequency of the excitation signal is low, the waveform of the displacement response of the rotor end is identical to one of the excitation signal. When the frequency of the excitation signal is smaller than 111240 rad/s (it is the first-order natural frequency of the rotor), it is considered to be low frequency. As the frequency of the excitation signal grows, the waveform of the displacement response becomes more different from one of the excitation signal. The first-order natural frequency of the rotor is the critical excitation frequency for the waveform change of the displacement response.

(2) The rise edge of the excitation voltage corresponds to a slow voltage change velocity, and its trailing edge corresponds to a rapid voltage change velocity in the opposite direction. Hence, the velocity response of the rotor end to the excitation voltage is the oscillation between two different velocities: one positive, and the other negative.

Under the excitation voltage, the rotor end velocity changes between two different values. When the rotor end velocity changes from one value to another, velocity oscillation occurs. As the frequency of the excitation signal is low, the time of the velocity oscillation is short, the time of the steady velocities is long. As the frequency of the excitation signal grows, the time of the velocity oscillation increases, and the time of the steady velocities is reduced. The steady velocity corresponding to the trailing edge first vanishes and then the steady velocity corresponding to the rising edge vanishes when the frequency of the excitation signal is getting to the first-order natural frequency of the rotor system.

Table 2. The parameters of the system.

R_1(mm)	R_2(mm)	h(mm)	l(mm)	E(GPa)	μ
12	13	1	12	119	0.9
l_p(mm)	b(mm)	h_p(mm)	e_{31}(C/m^2)	ρ(kg/m^3)	ξ_1
10	5	0.5	-5.2	8500	0.2

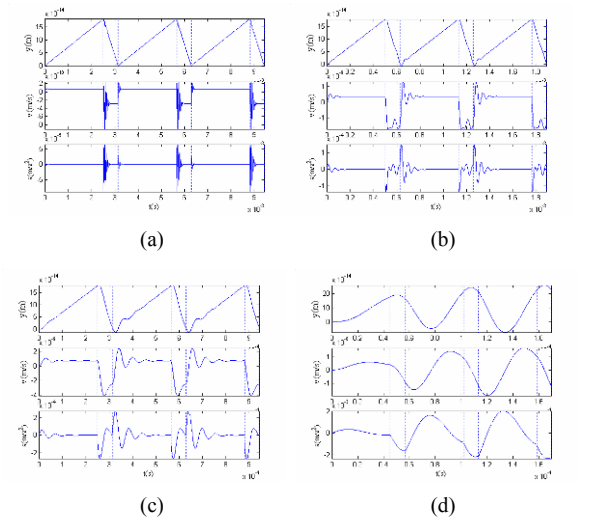

Fig. 5. The displacement, velocity and acceleration responses of the rotor to pulse signals.

(3) The steady values of the acceleration response corresponding to both rising edge and trailing edge of the excitation voltage are zero. When the excitation voltage changes from rising edge to the trailing edge or from trailing edge to the rising edge, the acceleration oscillation of the rotor occurs. The acceleration oscillation from rising edge to the trailing edge is more obvious than that from trailing edge to the rising edge.

As the frequency of the excitation signal grows, the steady acceleration corresponding to the trailing edge first vanishes, and then the steady acceleration corresponding to the rising edge vanishes when the frequency of the excitation signal is near to the first-order natural frequency of the rotor system.

The operating principle of the inertial piezoelectric rotary motor can be given as below. The friction torque of the motor bearing is

$$M_c = f\frac{d}{2}F, \tag{26}$$

where f is the rolling friction coefficient of the bearing, it is taken as 0.001~0.015; d is the inner diameter of the rolling

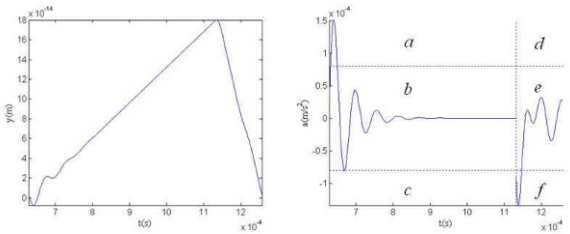

(a) Displacement (b) Acceleration

Fig. 6. The displacement and acceleration responses of the rotor end.

bearing; F is the load on the bearing, equal to the weight of the rotor.

The inertial torque applied to the rotor is

$$M = 2\left(m_h a l + m_l \frac{a}{4} l \right), \tag{27}$$

where m_h is the equivalent mass of the vibrator ring, m_l is the mass of the vibrator beam.

When the inertial torque applied to the rotor is larger than the friction torque of the motor bearing, the motor can rotate. Thus, the critical acceleration for the motor rotation is

$$a_0 = f \frac{d}{2} F \Big/ 2\left(m_h + \frac{m_l}{4} \right) l \,. \tag{28}$$

Fig. 6 shows the displacement and acceleration responses of the rotor end. In Fig. 6(b), there are six zones (*a*, *b*, *c*, *d*, *e* and *f*). The zones *a*, *c*, *d* and *f* correspond to the situation that the inertial torque applied to the rotor is larger than the friction torque of the motor bearing. The zones *b* and *e* correspond to the situation that the inertial torque applied to the rotor is smaller than the friction torque. The imaginary lines represent the critical acceleration a_0.

If the acceleration curve appears in the zone *a* or *d* (the acceleration is larger than the critical value), the inertial torque applied to the rotor is larger than the friction torque of the motor bearing. Hence, the motor rotates in one direction. If the acceleration curve appears in the zone *c* or *f* (the acceleration is larger than the critical value as well), the inertial torque applied to the rotor is larger than the friction torque of the motor bearing and the motor rotates in another direction. If the acceleration curve appears in the zone *b* or *e* (the acceleration is smaller than the critical value), the inertial torque applied to the rotor is smaller than the friction torque of the motor bearing. Thus, the motor does not rotate.

The area enclosed by the acceleration curve and the critical acceleration line in zone *a* represents the impulsive moment applied to the rotor in one direction. The area enclosed by the acceleration curve and the critical acceleration line in zone *f* represents the impulsive moment applied to the rotor in another direction. To make the motor rotate in one direction, the area enclosed by the acceleration curve and the critical acceleration line in zone *a* should be increased as large as possible, and the area enclosed by the acceleration curve and the critical acceleration line in zone f should be removed.

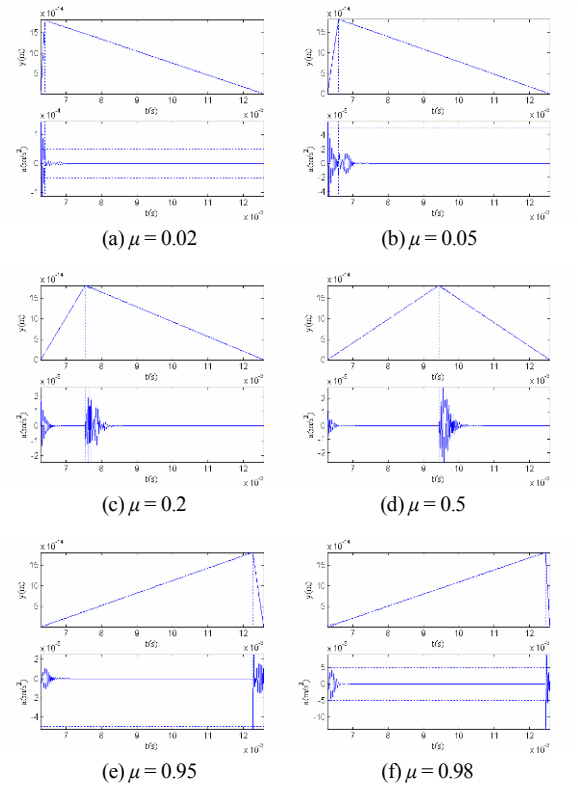

(a) $\mu = 0.02$ (b) $\mu = 0.05$

(c) $\mu = 0.2$ (d) $\mu = 0.5$

(e) $\mu = 0.95$ (f) $\mu = 0.98$

Fig. 7. The displacement and acceleration responses of the rotor end under different (ω = 10000 rad/s, $\xi_1 = 0.1$).

The impulsive moment applied to the rotor can be calculated by

$$v = \left| \int_{t_1}^{t_2} \left(a(t) - a_0 \right) dt \right|, \tag{29}$$

where t_1 and t_2 are two instant of the time, respectively, corresponding to the two crossing points of the critical acceleration line and the acceleration curve.

For different μ and different ξ_1, based on Eqs. (24) and (25), the displacement and acceleration responses of the rotor end to voltage excitation signals are investigated (see Figs. 7-9). They show:

(1) When the exciting frequency of the voltage signals is much smaller than the natural frequency of the rotor system($\omega \ll \omega_j$), the displacement and acceleration responses of the rotor end to voltage excitation signals are quite small and the impulsive moment applied to the rotor does not occur under the ratio range of $\mu = 0.1 \sim 0.9$.

For the ratio range of $0 < \mu < 0.1$, the slope ratio of the rising edge of the excitation voltage grows, and the impulsive moment applied to the rotor occurs. The motor can rotate in one direction.

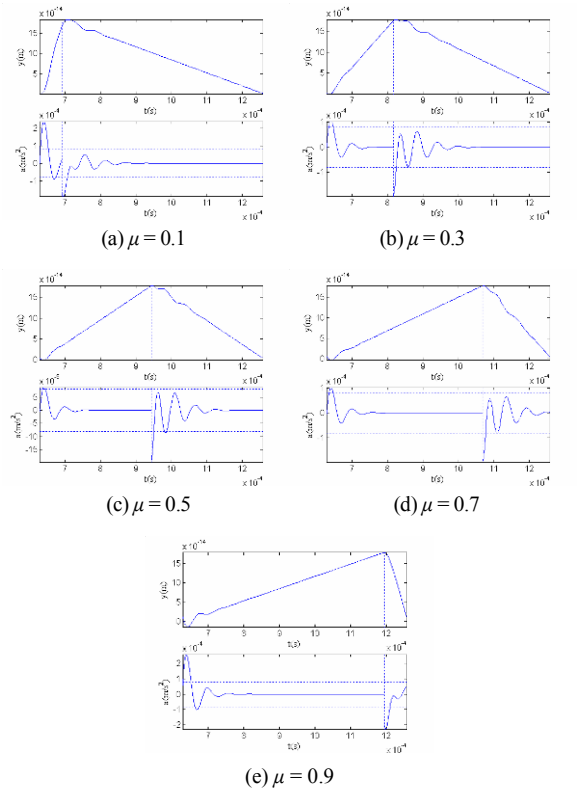

(a) $\mu = 0.1$ (b) $\mu = 0.3$ (c) $\mu = 0.5$ (d) $\mu = 0.7$ (e) $\mu = 0.9$

Fig. 8. The displacement and acceleration responses of the rotor end under different μ (ω = 10000 rad/s, ξ_1 = 0.3).

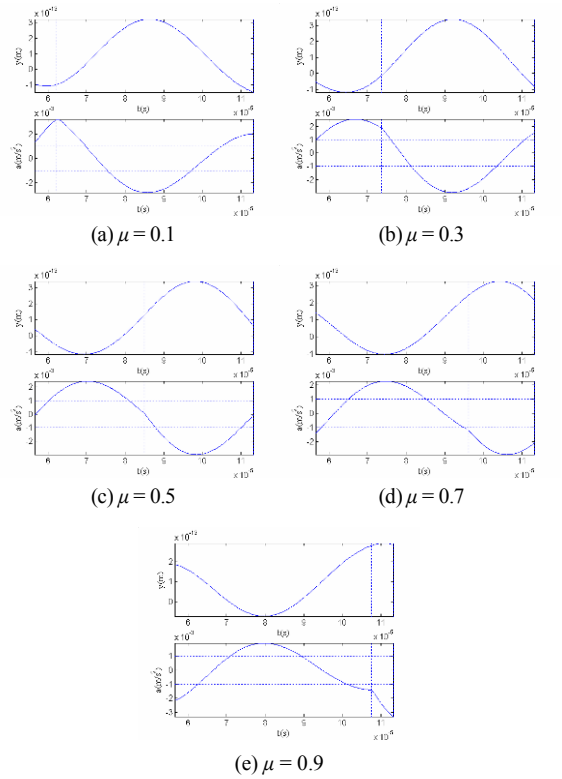

(a) $\mu = 0.1$ (b) $\mu = 0.3$ (c) $\mu = 0.5$ (d) $\mu = 0.7$ (e) $\mu = 0.9$

Fig. 9. The displacement and acceleration responses of the rotor end under different μ (ω = 10000 rad/s, ξ_1 = 0.1).

For the ratio range of $0.9 < \mu < 1$, the slope ratio of the trailing edge of the excitation voltage grows, and the impulsive moment applied to the rotor occurs. The motor can rotate in another direction.

(2) When the exciting frequency of the voltage signals is near to the natural frequency of the rotor system (10000 rad/s) and the damping coefficient is relatively large (ξ_1 = 0.3), the displacement and acceleration responses of the rotor end to voltage excitation signals are relatively large and the impulsive moment applied to the rotor occurs. However, for larger ratio range (μ = 0.1~0.4) or smaller ratio range (μ = 0.6~0.9), the impulsive moments applied to the rotor in positive and negative two directions are all relatively large. So, the rotation in one direction could not be obtained.

As the ratio μ is near to 0.5, the impulsive moment corresponding to the rising edge vanishes and the impulsive moment corresponding to the trailing edge remains. So, the rotation in one direction can be obtained.

(3) When the exciting frequency of the voltage signals is near to the natural frequency of the rotor system (10000 rad/s) and the damping coefficient is relatively small (ξ_1 = 0.1), the displacement and acceleration responses of the rotor end to voltage excitation signals are relatively large and a large impulsive moment applied to the rotor occurs. However, for different ratio μ (μ = 0.1~0.9), the impulsive moments applied to the rotor in positive and negative two directions are all relatively large. So, the rotation in one direction cannot be obtained.

Based on Eqs. (28) and (29), the effects of the geometric parameters of the motor rotor on the impulsive moment are also investigated (see Tables 3-5). Here, A = 400V, $\omega = 1\times10^4$. V is the integral value of Eq. (28); it represents the impulsive moment applied to the rotor. The Tables show:

(1) As the outer diameter R_2 of the rotor increases, the critical acceleration drops and the integral value v grows. So, the impulsive moment applied to the rotor grows with increasing the outer diameter R_2.

(2) As the length l of the rotor beam increases, the critical acceleration drops and the integral value v drops as well. As the length of the rotor beam increases, its stiffness decreases, which causes decrease of the acceleration of the rotor. So, the impulsive moment applied to the rotor grows with decreasing the length l of the rotor beam.

Thus, the impulsive moment applied to the rotor grows with decreasing the length l of the rotor beam.

(3) As the thickness h of the rotor beam increases, the critical acceleration grows, but the integral value v grows more obviously. So, the impulsive moment applied to the rotor grows with increasing the thickness h of the rotor beam.

Larger outer diameter and thickness of the rotor, smaller length of the rotor can give larger moment of inertia applied to the rotor.

Table 3. a_0 and v for different R_2.

R_2(m)	0.013	0.014	0.015	0.016	0.017
a_0(m/s^2)	0.0015	0.0012	0.00107	0.00096	0.00087
v(m/s)	0.77×10^{-9}	1.6×10^{-9}	2.15×10^{-9}	2.54×10^{-9}	2.93×10^{-9}

Table 4. a_0 and v for different l.

l(m)	0.012	0.013	0.014	0.015	0.016
a_0(m/s^2)	0.0015	0.0013	0.00115	0.001	0.0009
v(m/s)	0.77×10^{-9}	0.69×10^{-9}	0.62×10^{-9}	0.57×10^{-9}	0.48×10^{-9}

Table 5. a_0 and v for different h.

h(m)	0.001	0.0012	0.0014	0.0016	0.008
a_0(m/s^2)	0.0015	0.00155	0.0016	0.00165	0.0017
v(m/s)	0.77×10^{-9}	1.2×10^{-9}	1.5×10^{-9}	1.9×10^{-9}	2.1×10^{-9}

5. Conclusions

The equation of the voltage response on the piezo-ceramic bimorph and the dynamic equation of the rotor was determined. Using the equations, the responses of the voltage on the piezo-ceramic bimorph and the responses of the displacement, velocity and acceleration on the rotor to the sawtooth voltage excitation were investigated. The condition to make the motor rotate in one direction was discussed. The results show:

(1) The frequency of the excitation signal should be smaller than the first-order natural frequency of the rotor to obtain the same waveform of the voltage response on the piezo-ceramic bimorph as one of the excitation signal.

(2) Larger outer diameter and thickness of the rotor, smaller length of the rotor can give larger moment of inertia applied to the rotor.

Acknowledgment

This project is supported by National Natural Science Foundation of China (51275441).

Nomenclature

b : The effective width of the beam
h : The thickness of the beam
R_1 : The inter diameters of the rotor
R_2 : The outer diameters of the rotor
L_p : The length of the piezo-ceramic bimorph
t : Time
T : The period of the excitation signal
μ : The ratio of the rise time to the period
A : The peak voltage
V : The excitation voltage
V_R : The voltage on the resistance
V_C : The voltage on the piezo-ceramic bimorph
y : Transverse displacement of the beam
x : Length coordinate of the beam
ρ_l : Material density per unit length of the beam
E : Modulus of elasticity of the beam
I : The second moment of area of the beam
L_b : The length of the rotor
C_d : Damping coefficient
$\phi_i(x)$: Mode function
$q_i(t)$: Time function
E_3 : Electric-field intensity
e_{31} : Piezoelectric stress constant
c_{11}^E : Stiffness constant
ε : Strain
h_p : The thickness of the piezo-ceramic bimorph
m : Inertial mass
$\mathbf{M}$: The mass matrix
$\mathbf{K}$: The stiffness matrix
$\mathbf{C}$: The damping matrix
x_a, x_b : The average positions of the piezo-ceramic bimorphs
ω_j : The jth natural frequency of the rotor
ξ_j : The relative damping coefficient
f : The rolling friction coefficient of the bearing
d : The inner diameter of the rolling bearing
F : The load on the bearing
m_h : The equivalent mass of the vibrator ring
m_l : The mass of the vibrator beam
$t_{1,2}$: Two instant of the time

References

[1] T. Sashida and T. Kinjo, *An introduction to ultrasonic motors*, Clarendon Press, Oxford (1993).
[2] S. Ueha, Y. Tomikawa, M. Kurosawa and N. Nakamura, *Ultrasonic motors: Theory and applications*, Clarendon Press, Oxford (1993).
[3] K. Nakamura and S. Uhea, Potential ability of ultrasonic motors: a discussion focused on the friction control mechanism, *Electronics and Communication in Japan*, 281 (4) (1998) 57-68.
[4] T. Morita, Miniature piezoelectric motors, *Sensors and actuators A*, 103 (2003) 291-300.
[5] K. Hideki, H. Yasuo, K. Hitoshi and H. Toshiro, Positioning and measurement using a crystalline lattice reference scale--A feasibility study of STM application to MEMS, *IEEE Micro Electro Mechanical Systems-An Investigation of Micro Structures, Sensors, Actuators, Machines* (1990) 197-202.
[6] K. Hideki, H. Yasuo, K. Hitoshi and H. Toshiro, Crystalline lattice for metrology and positioning control, *Proceedings of IEEE Micro Electro Mechanical Systems* (1991) 239-244.
[7] A. Bergander, J. M. Breguet, C. Schmitt and R. Clavel, Micropositioners for microscopy applications based on the stick-slip effect, *Proceedings of the International Symposium on Micro Machine and Human Science* (2000) 213-216.
[8] J. M. Breguet and R. Clavel, Stick and slip actuators: Design, control, performances and applications, *Proceedings of the*

International Symposium on Micromechatronics and Human Science (1998) 89-95.

[9] R. Yoshida, Y. Okamoto and H. Okada, Development of smooth impact drive mechanism (2nd report) - Optimization of waveform of driving voltage, *Seimitsu Kogaku Kaishi/Journal of the Japan Society for Precision Engineering*, 68 (4) (2002) 536.

[10] Y. Suzuki, K. Tani and T. Sakuhara, Development of a new type piezoelectric micromotor, *Sensors and Actuators, A: Physical*, 83 (1) (2000) 244-248.

[11] Z. Boumous, S. Belkhiat and F. Z. Kebbab, Effect of shearing deformation on the transient response of a traveling wave ultrasonic motor, *Sensors and Actuators, A: Physical*, 150 (2) (2009) 243-250.

[12] P. Simone, S. Rosario and M. Alberto, Evaluation of the effect of preload force on resonance frequencies for a traveling wave ultrasonic motor, *IEEE Transactions on Ultrasonics, Ferroelectrics, and Frequency Control*, 53 (4) (2006) 746-752.

[13] H. Frayssignes and R. Briot, Traveling wave ultrasonic motor: Coupling effects in free stator, *Ultrasonics*, 41 (2) (2003) 89-95.

[14] L. Xu and J. Xing, An inertial piezoelectric rotary motor, *J. of Mechanical Engineering Science*, 224 (C6) (2010) 1165-1171.

[15] J. Xing and L. Xu, Torque for an inertial piezoelectric rotary motor, *The Scientific World Journal* (2013) Article ID 854126.

[16] H. Baruh, *Analytical dynamics*, McGraw-Hill, New York (1999) 620.

[17] W. Heywang, K. Lubitz and W. Wersing, *Piezoelectricity: evolution and future of a technology*, Peking: Peking University Press (2012).

Lizhong Xu is a full Professor in machine design and theory at the Yanshan University, China. He received his Ph.D. in machine design and theory from Yanshan University in 1999. His primary research interests are in the area of mechanical transmission and electro-mechanical integrated system.

Jichun Xing is a lecturer in machine design and theory at the Yanshan University, China. He received his Ph.D. in machine design and theory from Yanshan University in 2012. His primary research interests are in the area of mechanical transmission and piezo-electric motor.